NASA Technical Memorandum 4806

Flight Demonstration of a Shock Location Sensor Using Constant Voltage Hot-Film Anemometry

Timothy R. Moes
Dryden Flight Research Center
Edwards, California

Garimella R. Sarma and Siva M. Mangalam
Tao of Systems Integration, Inc.
Hampton, Virginia

National Aeronautics and
Space Administration

Office of Management

Scientific and Technical
Information Program

1997

FLIGHT DEMONSTRATION OF A SHOCK LOCATION SENSOR USING CONSTANT VOLTAGE HOT-FILM ANEMOMETRY

Timothy R. Moes*
NASA Dryden Flight Research Center
Edwards, California

Garimella R. Sarma† and Siva M. Mangalam‡
Tao Systems
Hampton, Virginia

Abstract

Flight tests have demonstrated the effectiveness of an array of hot-film sensors using constant voltage anemometry to determine shock position on a wing or aircraft surface at transonic speeds. Flights were conducted at the NASA Dryden Flight Research Center using the F-15B aircraft and Flight Test Fixture (FTF). A modified NACA 0021 airfoil was attached to the side of the FTF, and its upper surface was instrumented to correlate shock position with pressure and hot-film sensors. In the vicinity of the shock-induced pressure rise, test results consistently showed the presence of a minimum voltage in the hot-film anemometer outputs. Comparing these results with previous investigations indicate that hot-film anemometry can identify the location of the shock-induced boundary layer separation. The flow separation occurred slightly forward of the shock-induced pressure rise for a laminar boundary layer and slightly aft of the start of the pressure rise when the boundary layer was tripped near the airfoil leading edge. Both minimum mean output and phase reversal analyses were used to identify the shock location.

Nomenclature

c	airfoil chord length, 10 in.
CFD	computational fluid dynamics
C_p	pressure coefficient, $(p - p_s)/\bar{q}$
C_p^*	pressure coefficient corresponding to local sonic velocity
CVA	constant voltage anemometer
FTF	Flight Test Fixture (NASA Dryden)
I_s	hot-film current
NACA	National Advisory Committee on Aeronautics
p	pressure on the airfoil surface
p_s	ambient pressure
PSD	power spectral density
$\bar{q}$	dynamic pressure
r	boundary layer reattachment location
R_1, R_2, R_F	circuit resistances

*Aerospace Engineer, 805-258-3054
†Research Engineer, 757-827-4434
‡Research Engineer, 757-827-4434

R_s	hot-film resistance
s	boundary layer separation location
V_{DC}	circuit input voltage
V_o	circuit output voltage
V_s	hot-film voltage
x	distance from leading edge of the airfoil, in.
x/c	nondimensional chord location
α	temperature coefficient of resistance, approx. 0.004 Ω/Ω/°C
ΔR_s	change from the reference condition of hot-film resistance
ΔT	change from the reference condition of hot-film temperature, °C
ΔV_o	change from the reference condition of circuit output voltage

Introduction

Because of the complex interaction of the shock with the boundary layer, transonic shock location and transonic aerodynamic characteristics in general are highly dependent on Reynolds number. Experience has shown it difficult to correctly simulate the full-scale transonic shock location in wind tunnels, which has led to significant errors in predicting aircraft transonic performance and handling qualities.[1] Consequently, measurement of transonic shock locations on a full-scale aircraft is desired to correlate results with computational fluid dynamics (CFD) and wind-tunnel predictions.

This paper presents results from flight tests that demonstrated the effectiveness of an array of hot films to sense shock location. Constant voltage anemometry (CVA)[2–7] was used in conjunction with the hot films in the first phase of a study to develop a real-time sensor that can locate a steady or rapidly moving shock. Once developed, this sensor could provide researchers an additional tool to improve CFD results and techniques for transonic wind-tunnel testing.

Another potential application of this sensor is to determine shock impingement location. Shock impingement is also Reynolds-number dependent because the shock impinges a boundary layer. This application includes inlet shock location sensing for supersonic cruise vehicles. Information from the sensor could be fed back in real time to a variable geometry inlet control system designed to optimize engine inlet performance.

Traditionally, pressure measurements have been used to estimate shock location. Hot films are considered a potential alternative to pressure measurements for shock-location sensing for several reasons. These reasons include easier installation and operation, higher frequency response, and better spatial resolution as, in many cases, the hot films can be placed closer together. Hot films can also provide more information on the interaction of the shock with the boundary layer. This information includes boundary-layer characteristics such as turbulence level and separation and reattachment locations.

Flight tests were conducted using the NASA Dryden Flight Research Center's F-15B Flight Test Fixture (FTF) at an altitude of 20,000 ft and Mach numbers 0.68 through 0.80. A low-aspect-ratio wing section using a modified NACA 0021 airfoil[8] was attached to the side of the FTF and instrumented with

upper surface pressure and hot-film sensors. The hot-film outputs were correlated to the shock location estimates inferred from the pressure measurements. Both laminar and tripped boundary layers were investigated. Flight test results and a proposal for a real-time sensor approach are presented.

Note that use of trade names or names of manufacturers in this document does not constitute an official endorsement of such products or manufacturers, either expressed or implied, by the National Aeronautics and Space Administration.

Experiment Description

Flight Test Fixture

The FTF was used to mount and flight test this experiment. Installed on the lower fuselage centerline of the NASA F-15B aircraft (fig. 1), the FTF uses the same hardware attachment points as the standard centerline fuel tank. The FTF was created as a testbed for generic aerodynamics research[9] and is 107 in. long, 32 in. high, and 8 in. wide with a 12° elliptical nose section and blunt trailing edge. A noseboom is mounted at the leading edge of the FTF to measure pitot and static pressures and local flow angles.

For this experiment, a total temperature probe was installed on the left side of the FTF near the trailing edge. The test article for this experiment was mounted on the left side of the FTF (fig. 2), approximately 87 in. aft of the leading edge and 9.6 in. from the bottom. Data were telemetered to a ground control room for real-time monitoring and recording.

Test Article

The aluminum test article (fig. 3) consisted of a low-aspect-ratio wing with a modified

EC96-43815-02

Figure 1. The F15-B in flight with the FTF and test article installed.

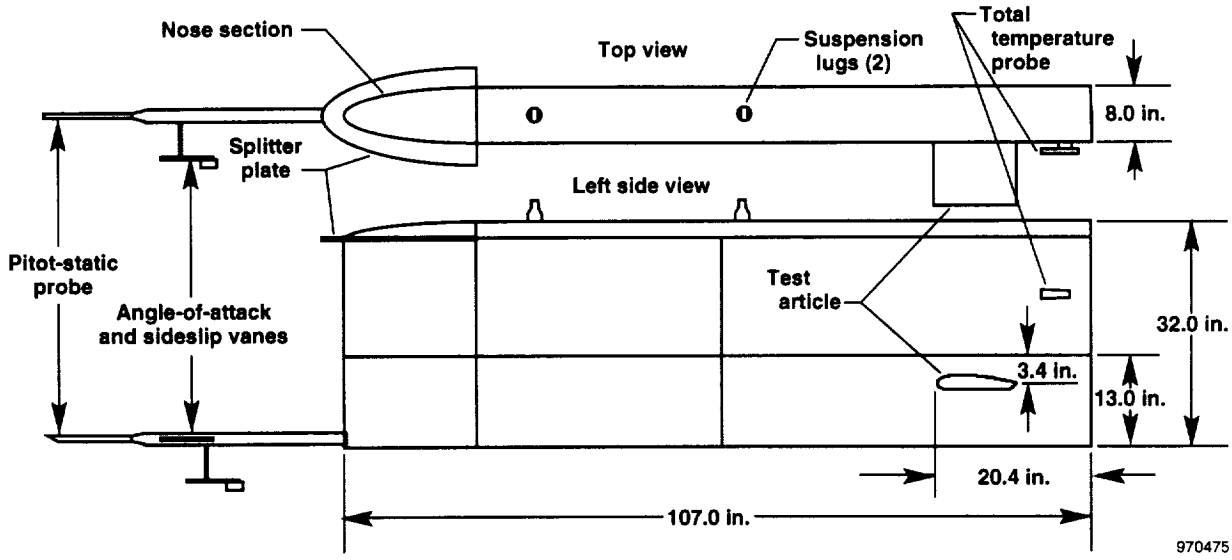

Figure 2. The FTF with the test article.

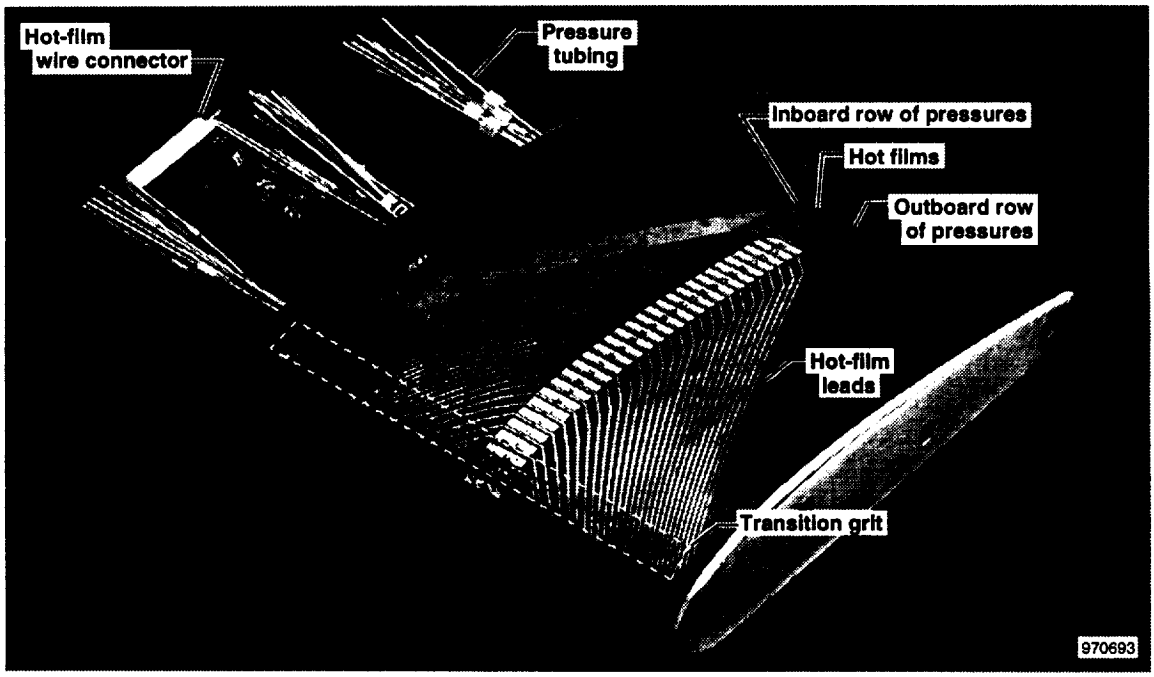

Figure 3. The test article showing upper surface instrumentation and the grit strip.

NACA 0021 airfoil section. The unswept wing had an 8.5 in. span and a 10 in. chord. The lower airfoil surface was flattened and the trailing edge was blunted to allow internal installation of pressure ports and the routing of electrical leads from the surface-mounted hot films. Sixty-two flush pressure ports were installed on the upper surface as shown in figure 4.

Stainless steel tubing with internal diameter of 0.031 in. was used to plumb the pressure

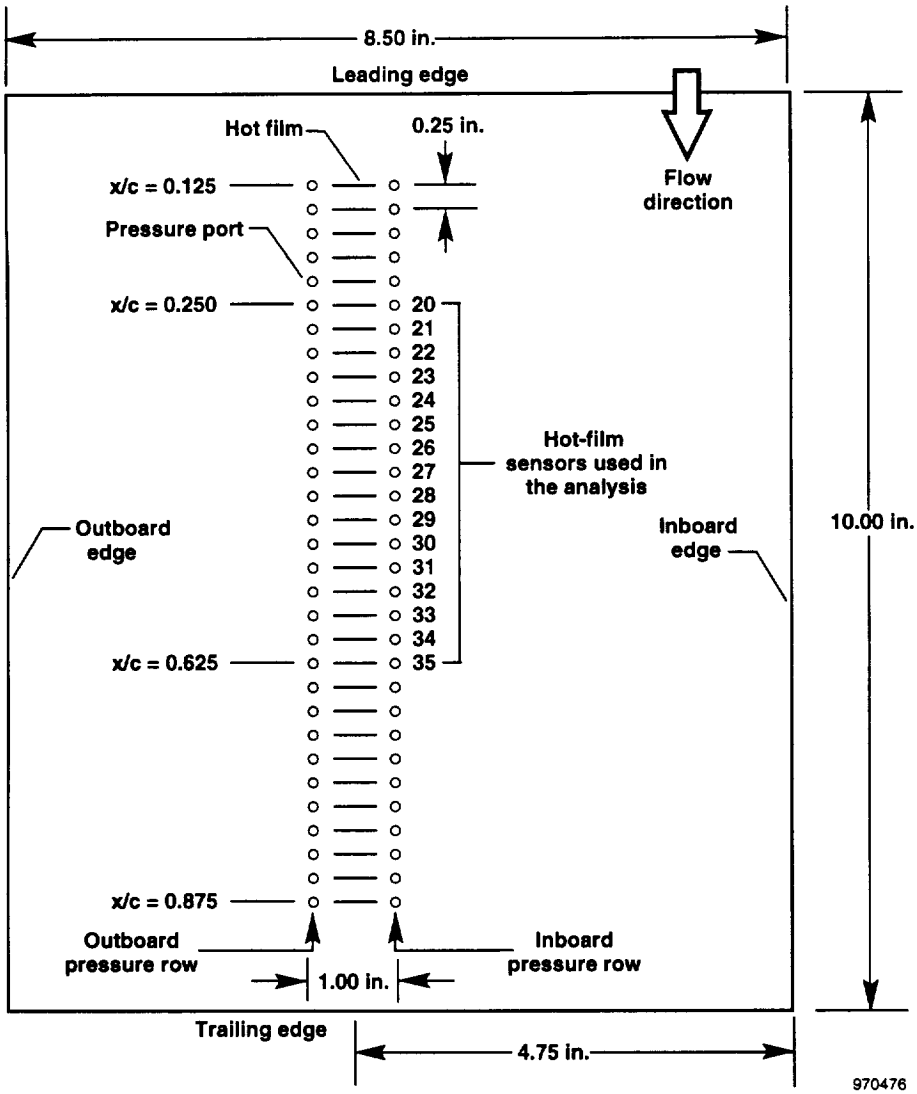

Figure 4. Upper surface instrumentation on the test article.

ports. The pressure tubing was routed into the FTF and connected to flexible tubing (0.055 in. internal diameter) once inside the FTF. A polymide sheet containing the hot films and associated wire leads covered the entire upper surface of the airfoil. Pressure port holes were drilled through this sheet.

The actual hot-film sensors were placed at the same chord locations as the pressures, as seen in figure 4. The electrical leads from the hot-film sensors were routed along the top of the test article outward and forward and then around the leading edge and into the test article. The leads were then directed into the FTF and connected to the CVA circuits.

Instrumentation

Air Data

The FTF pitot-static measurements were corrected for position error to obtain

freestream measurements of Mach, ambient pressure, and dynamic pressure. The FTF total temperature probe was used with Mach number to obtain freestream ambient temperature. An angle-of-attack vane was also installed on the FTF noseboom and provided local angle of attack forward of the FTF. The angle of attack at the test article, however, was appreciably different from that forward of the FTF because of fuselage flow straightening.[9] Consequently, no direct measurements of local angle of attack were made at the test article. All air data parameters were measured and recorded at 52 Hz.

Pressure Measurements

Pressure measurements from the upper surface were obtained using two 32-port electronically scanned pressure transducer modules. These modules measured the difference between the surface pressure and a reference pressure. The reference pressure was from the static pressure source on the FTF noseboom and measured using a 0–19 psia 20-bit digital pressure transducer. The forward port pressures were measured with a ±10 psid module, and the aft pressure ports were measured with a ±5 psid module.

Approximately 3 ft of pressure tubing were used between the surface port and the transducer, and consequently pneumatic lag was less than 0.02 sec. This situation was not a problem for these tests because of the quasi-steady-state nature of the flight test maneuvers. Pressure data were measured and recorded at 52 Hz.

Hot-Film Anemometry

The multi-element, hot-film sensor sheet used in these tests consisted of an array of 45 nickel elements (1 mm long, 0.12 mm wide, and 0.25 μm thick) on a polymide substrate. The elements were attached to 13-μm thick, copper-coated nickel leads that were routed, as shown in figure 3, to the airfoil lower surface.

The sensor leads were soldered onto 33-gauge wires that were routed through a narrow slot on the lower surface into the airfoil. Coaxial cables connected these wires to a bank of CVAs inside the FTF. The unheated resistance of the sensor elements was a nominal 10 Ω on the ground and dropped to approximately 8.5 Ω at 20,000 ft altitude, where the ambient temperature was approximately 11 °F.

Appendix A describes the operation of the hot-film anemometry. The voltage across the hot film remains constant and thus is referred to as constant voltage anemometry. However, the measured output of the CVA circuit is a voltage that directly relates to the temperature of the hot film. The output voltages measured from the multiple hot-film sensors were pre-sample filtered with a 3-pole Butterworth filter having a low-pass rolloff frequency of 503 Hz.

The data were telemetered to the ground station and recorded at 1667 Hz. For each flight test, only 16 of the hot films were operational. Between flights the anemometry system could be reconfigured to measure a different set of 16 hot-film sensors. Hot films 20 through 35 were used for the results in this paper.

Test Approach

Flight data were obtained at an altitude of approximately 20,000 ft during stabilized flight, angle-of-attack sweeps, and acceleration and deceleration

maneuvers. Before collecting data, the pilot reset the current in the hot films and auto-zeroed the circuit output voltage at 20,000 ft.

To properly configure the system, the reset and auto-zeroing were done at a Mach number less than the test Mach numbers (typically Mach 0.50) and only once in the flight. The stabilized flight points consisted of approximately 20 sec of constant altitude and Mach flight. The angle-of-attack sweeps were typically ±2° in amplitude and were performed at Mach numbers between 0.68 and 0.80.

Acceleration and deceleration maneuvers were performed at constant altitude between Mach 0.6 and 0.8 with chord Reynolds number varied between 1.8 and 2.5 million. The flow was expected to be laminar before any transonic shock interaction for the low chord Reynolds numbers tested.

It was desired to obtain data with both laminar and turbulent boundary layers because the shock and boundary layer interactions depend on the condition of the boundary layer.[10–11] For some flights, grains of 0.02-in. maximum diameter grit were added at approximately 5 to 8 percent chord to transition the boundary layer and therefore obtain data with a tripped boundary layer upstream of the shock location.

Results and Discussion

Stabilized flight data were obtained at 20,000 ft altitude and at Mach numbers of 0.68, 0.70, 0.72, 0.74, 0.76, 0.78, and 0.80 with a laminar boundary layer upstream of the shock. One stabilized test point at Mach 0.70 was obtained with the grit strip installed. Hot-film and pressure measurements showed that the grit strip made a significant effect; however, it was unknown whether it created fully turbulent flow upstream of the shock. Hence, when discussing results using the grit strip, this paper refers to the boundary layer as *tripped* and not turbulent.

As representative cases, the pressure distribution and hot-film voltage outputs are plotted in figure 5 for data at Mach 0.70. Figure 5(a) shows data for a laminar boundary layer, and figure 5(b) shows data for a tripped boundary layer.

From the pressure distributions a difference between the two rows of pressure measurements can be seen. The difference is largest in the region near the large pressure rise associated with the transonic shock. The differences are seen at each tested Mach number and are caused by a 3D flow on the test article. Note that the boundary layer from the FTF at the test article is approximately 1.5 in. thick.[9] The critical pressure coefficient, C_p^*, also shown on figure 5, is defined as the pressure coefficient corresponding to sonic velocity.[10]

For this paper, the shock location is inferred from the pressure measurements to be where the shock-induced rapid pressure rise begins. This definition is consistent with others in the literature.[10,12] The location is somewhat subjective because of the differences in the inboard and outboard rows of pressure measurements. For the laminar boundary layer case shown in figure 5(a), the rapid pressure rise begins at approximately x/c = 0.325 (near hot film 23), whereas for the tripped boundary layer case shown in figure 5(b) the rapid pressure rise begins at approximately x/c = 0.275 (near hot film 21).

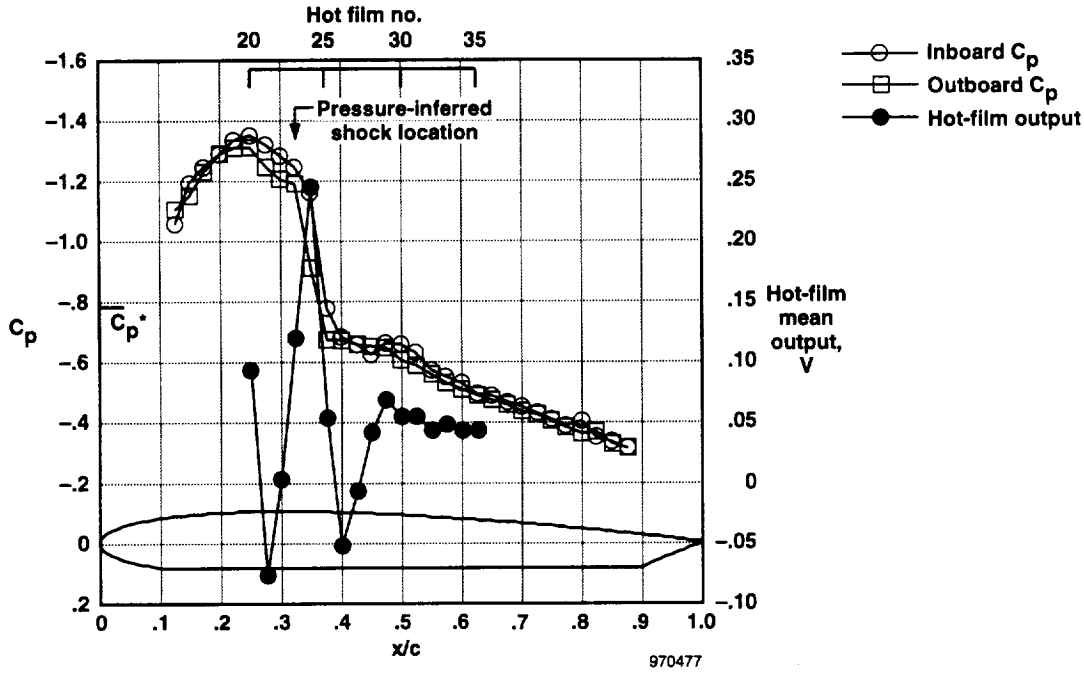

(a) Laminar boundary layer.

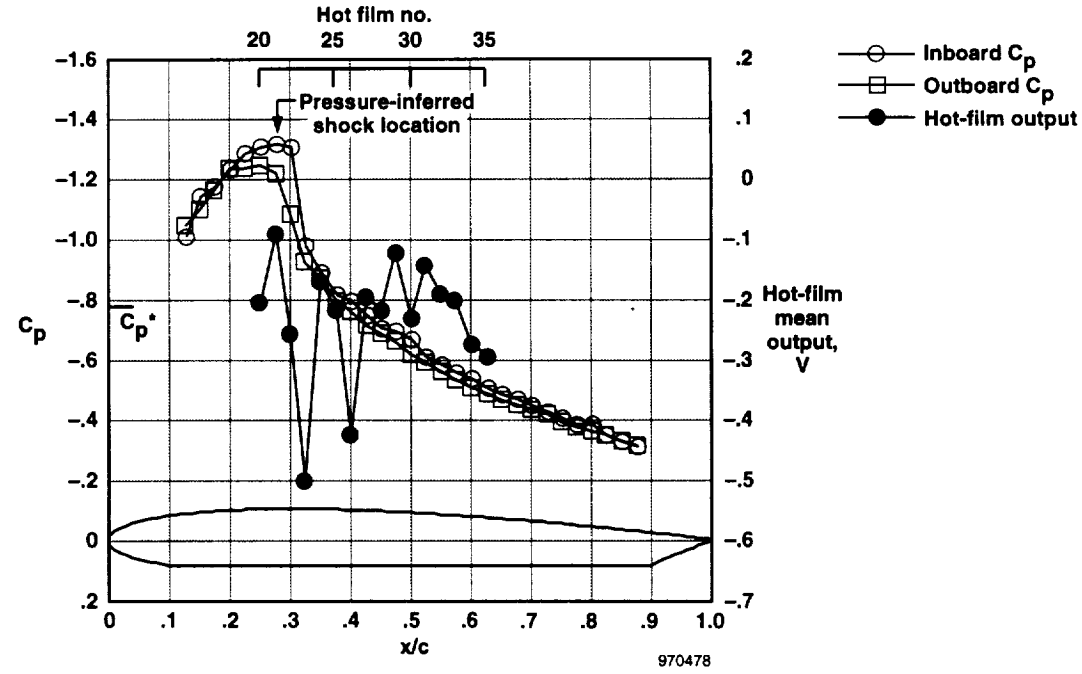

(b) Tripped boundary layer.

Figure 5. Pressure and hot-film mean voltage distributions for stabilized flight at Mach 0.7.

Minimum Mean Voltage Outputs

Figures 5(a) and 5(b) also show mean voltage outputs of hot films for Mach number 0.70. Mean voltages were obtained by averaging 1 sec of stabilized flight data. Before the test points, the CVA outputs were zeroed at Mach 0.50 for the laminar flow case and at Mach 0.65 for the tripped flow case. The auto-zero function did not completely zero the hot films, with as much as 0.08 V offset remaining. Therefore, postflight zeroing was done before analyzing the data. Note the location of the hot film with the minimum voltage output.

For the laminar boundary layer case shown in figure 5(a), hot film 21 (x/c = 0.275) outputs the minimum value. Hot film 21 is forward of the rapid pressure rise (x/c = 0.325) and aft of the minimum pressure location (x/c = 0.250). For the tripped boundary layer case shown in figure 5(b), hot film 23 (x/c = 0.325) outputs the minimum value. Hot film 23 is aft of the rapid pressure rise (x/c = 0.275).

Analysis of pressure and hot-film data at other Mach numbers showed similar results. Locations of hot-film minimum mean voltages for laminar boundary layer cases are correlated with the pressure-inferred shock locations as a function of Mach number in figure 6. At all Mach numbers, the location of the hot-film minimum is slightly forward of the pressure-inferred shock location.

As mentioned previously, stabilized data for the tripped boundary layer case were only obtained at Mach 0.70. Hot-film data were obtained, however, for a tripped boundary layer during a level acceleration maneuver. Only hot films 23, 24, 25, 27, 28, and 30 were operational, and the acceleration was approximately 3 kn/sec.

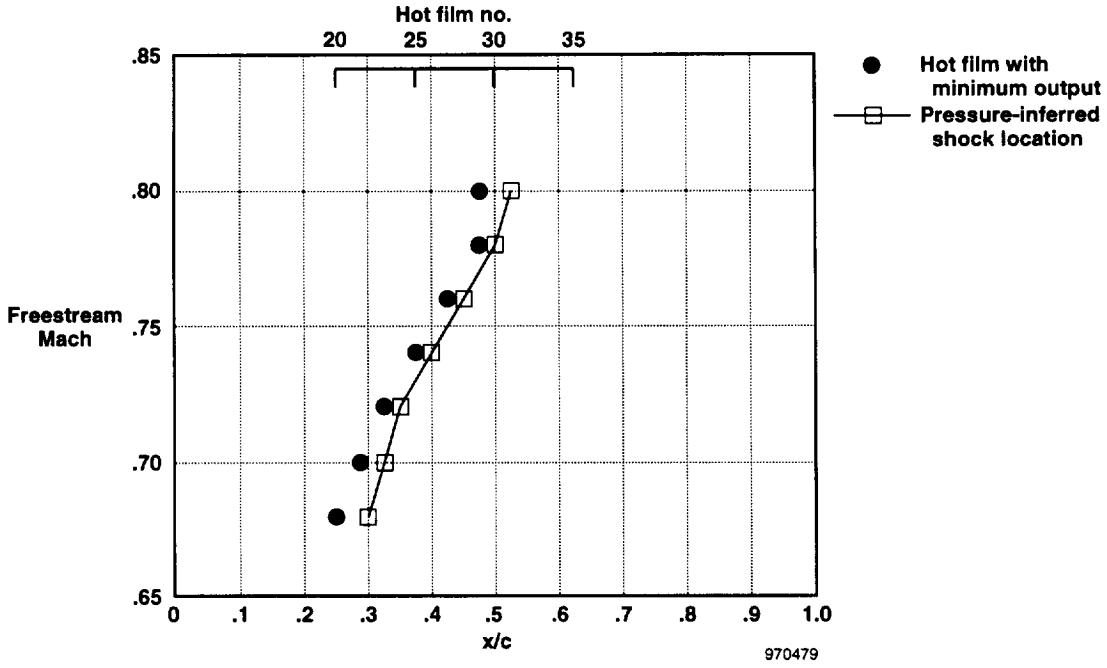

Figure 6. Comparison of hot-film minimum voltages with pressure-inferred shock locations for a laminar boundary layer.

Figure 7 shows the Mach number at which these hot films produced the minimum value of output during the acceleration. Figure 7 also shows the pressure-inferred shock location. At all Mach numbers, the hot film with the minimum output voltage occurs aft of the pressure-inferred shock location. This trend was also seen during a level deceleration maneuver.

Angle-of-attack sweeps were made to demonstrate the ability to track the shock location during a dynamic maneuver. Sweeps of approximately ±2° were made at various Mach numbers.

Figure 8 shows a time history of a quasi-steady-state test point followed by an angle-of-attack sweep at Mach 0.70. For this case a laminar boundary layer is forward of the shock. During the first 20 sec of the maneuver, the angle of attack is held constant while the Mach number changes slightly. The angle-of-attack sweep is shown in the last 20 sec. Only four hot-film outputs are shown for simplicity.

For the most part, hot film 22 has the minimum voltage output for the first 20 sec of the maneuver. As the aircraft decreased angle of attack, hot film 23 has the minimum voltage output. As the aircraft pulled up, hot film 22 has the minimum voltage output, then hot film 21, and then hot film 20 at the peak angle of attack. Pushing over to trim angle of attack, hot film 22 again has the minimum voltage output.

This movement of the minimum voltage output is consistent with the movement of the shock shown in figure 9. Pressure distributions in figure 9 clearly show the pressure rise moving aft during the pushover, moving forward during the pullup, and then moving back to the original position.

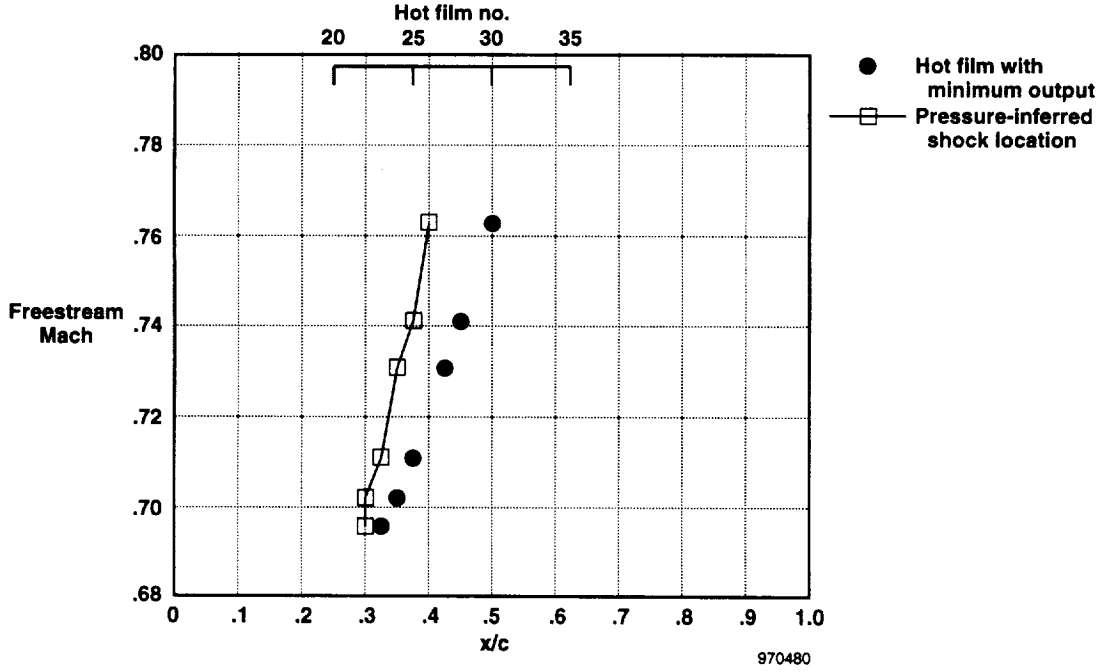

Figure 7. Comparison of hot-film minimum voltages with pressure-inferred shock locations for a tripped boundary layer.

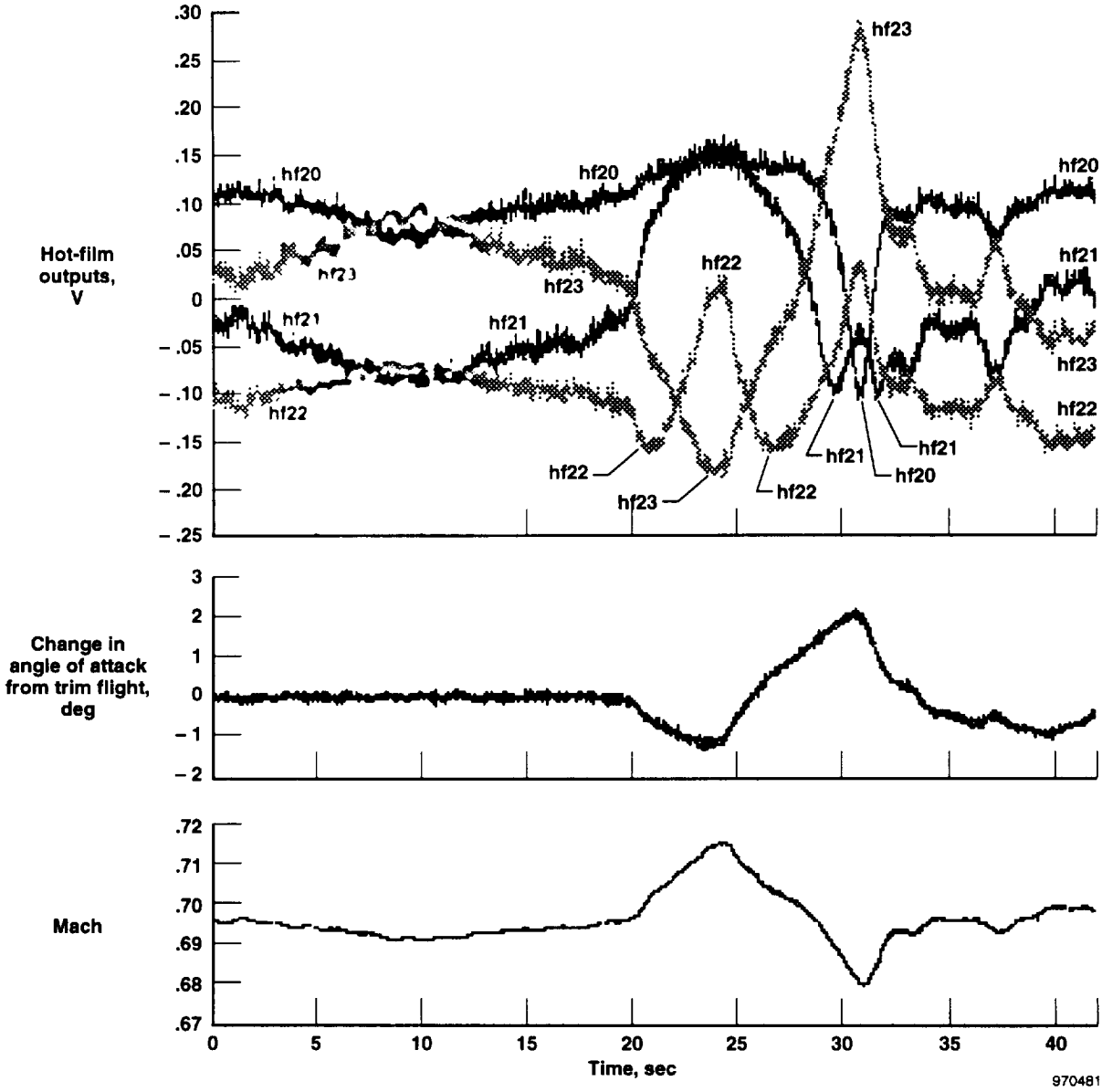

Figure 8. Time history of stabilized flight and an angle-of-attack sweep at Mach 0.7.

Phase Reversal

During the first 20 sec of the time history in figure 8, these hot-film outputs are highly sensitive to Mach-number variations. Hot films 20 and 21 are in phase with Mach number (i.e., decreasing in output as Mach number decreases and increasing in output as Mach number increases). Hot films 22 and 23 show just the opposite response and are approximately 180° out of phase with Mach number and are therefore out of phase with hot films 20 and 21.

As appendix B describes, the phase reversal between hot films 21 and 22 can be an indicator of the shock location. We have hypothesized from figure 8 that the

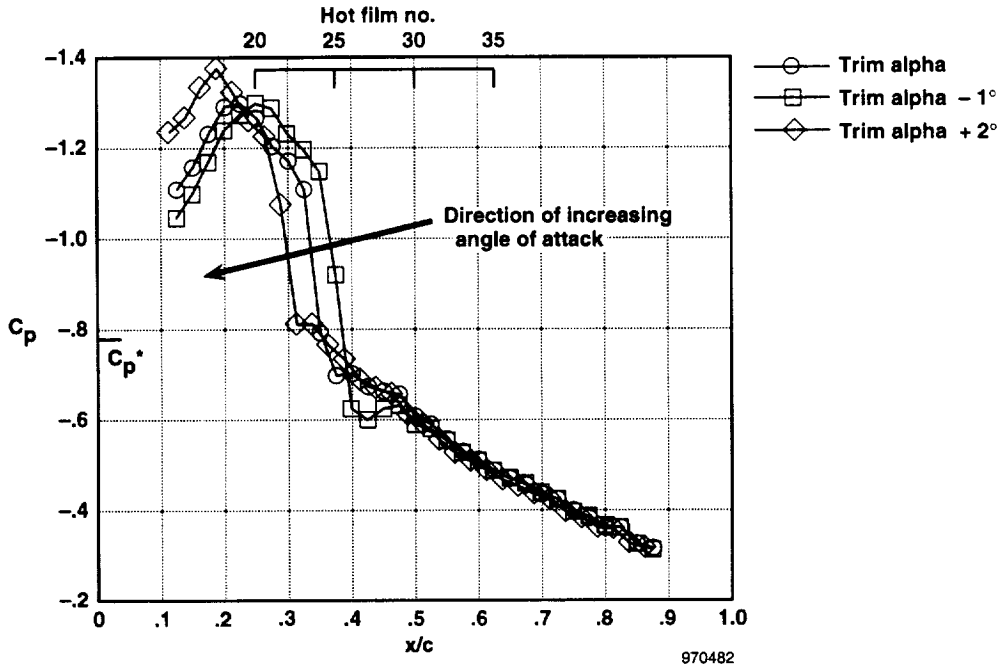

Figure 9. Pressure distributions during an angle-of-attack sweep at Mach 0.7.

shock is near hot films 21 and 22 because the minimum mean voltage output varies between these hot films for the first 20 sec of the maneuver. The phase reversal concept also indicates this hypothesis because hot films 21 and 22 are out of phase with each other.

During the angle-of-attack sweep, we can see that hot films 20 and 23 are basically out of phase with each other the entire time, indicating that the shock-induced phenomena is between them. Another interesting feature from this low-frequency analysis is that hot film 22 exhibits a frequency approximately twice that of the other hot films during the angle-of-attack sweep. This feature indicates that the shock oscillates around hot film 22 during this maneuver.

Spectral analysis can identify phase reversal. As stated previously, the hot-film data were pre-sample, low-pass filtered with a rolloff frequency of 503 Hz and recorded at 1667 Hz. A 6-sec portion of the constant angle-of-attack data from figure 8 was analyzed using Fourier transforms with resulting phase angles from hot films 20 through 23 shown in figure 10.

At low frequencies clearly hot films 20 and 21 are roughly 180° out of phase from hot films 22 and 23. At higher frequencies the differences in phase angles are not distinguishable because of spectral noise. Phase reversal about the hot film with the minimum output was seen using this technique at all Mach numbers tested. However, additional low-pass filtering of the signals was required at the higher Mach numbers before using the Fourier transform phase angle analysis.

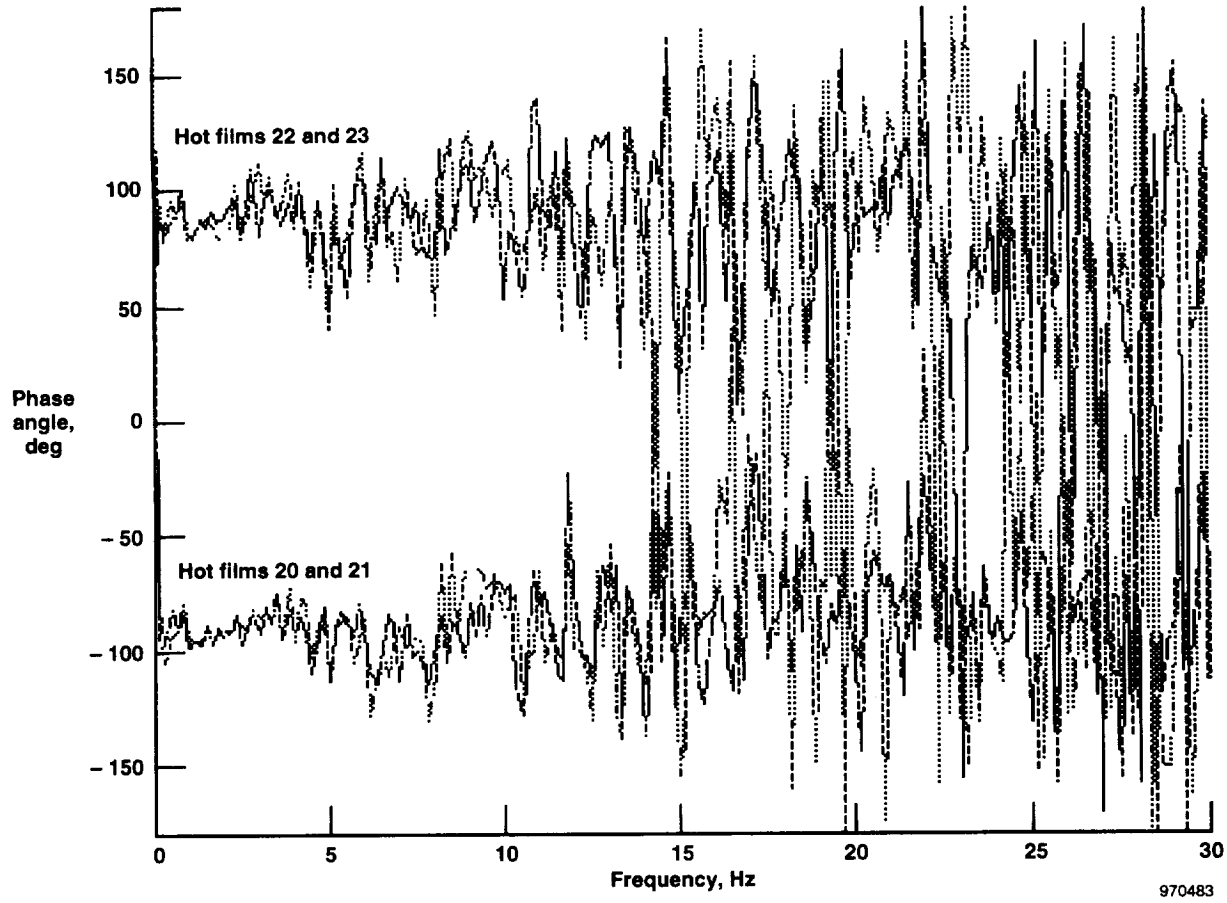

Figure 10. Phase angles from hot films 20 through 23 during a Mach 0.7 quasi-steady-state test point.

Flow Structure

These flight tests provide an initial look into transonic shock location detection using hot films with CVA. The results show that both minimum mean voltage and phase reversal are potential indicators of the shock location. The hot films, of course, are surface measurements that identify features in the complex off-surface interactions between the shock and the boundary layer.

Numerous authors have described shock and boundary layer interactions in detail.[10,13,14] Typically, the adverse pressure gradient induced by the shock would cause local separation of the boundary-layer flow. The location of the separation is related to the condition of the boundary layer. As discussed in appendix A, the hot films in the present study were operated at current levels sufficient to measure velocity fluctuations over the surface and therefore to identify separated flow regions.

Previous hot-film experiments[4] have shown that flow separation in the boundary would lead to a minimum output in a hot-film array because of reduced convective heat transfer. Consequently, it was hypothesized

that the primary factor creating a local minimum in the hot-film array voltages was boundary layer flow separation induced by the adverse pressure gradient associated with the shock. The flow separation begins near the location of the hot film with the minimum output.

At some transonic Mach numbers two distinct minimums occur in the hot-film outputs as seen in figure 5 This second minimum is suspected to indicate flow reattachment. Both separation and reattachment points would be in regions of reversed flows and hence a stagnation point would occur and convective heat transfer would be diminished This situation would cause the hot-films to heat up and the output voltage to drop at these locations.

A comparison of hot-film output minimums with the pressure distributions in figure 5 indicates that the separation region began farther upstream of the shock when the flow was laminar than when it was tripped. This result is consistent with the fact that turbulent boundary layers are more difficult to separate.

Another observation from figure 5 is that the hypothesized separation and reattachment are farther apart for the laminar boundary layer case. The separation and reattachment points are separated by 12.5-percent chord for the laminar flow case and only 7.5-percent of the chord for the tripped flow case. Figure 11 graphically displays the shock and boundary layer features that have been hypothesized from the hot film and pressure distributions.

Further evidence of this separated flow region can be seen in the power spectral densities (PSDs) of the hot films. PSDs of three normalized hot-film signals and normalized angle of attack are shown in figure 12 for data obtained with a laminar boundary layer at Mach 0.70. The signals were normalized by dividing the signal by its standard deviation before obtaining the PSD. Hot-film minimums were measured at hot films 21 and 26, indicating a separated flow region between them (fig. 5(a)). PSD analysis of the noseboom angle-of-attack signal showed a peak near 13 Hz at this Mach number because of an unknown source.

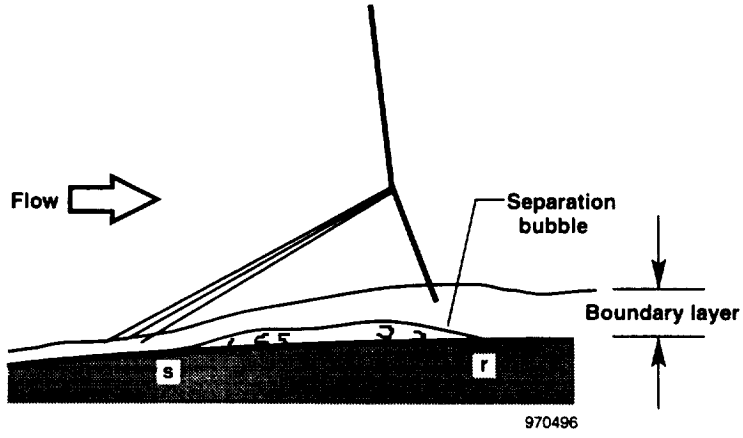

(a) Laminar flow upstream of the shock.

Figure 11. Hypothesized flow structure near the shock.

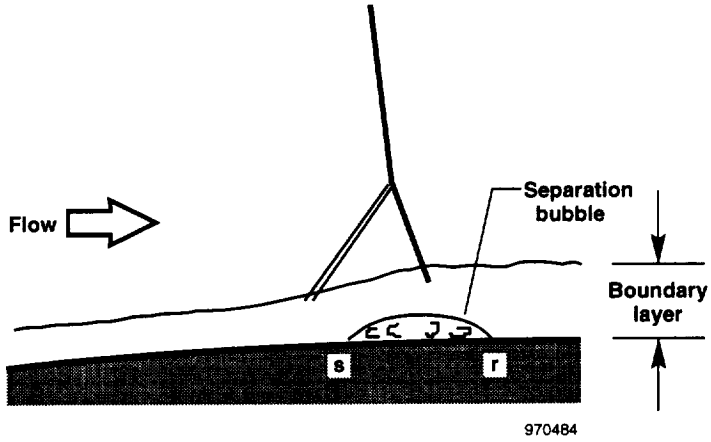

(b) Tripped flow upstream of the shock.

Figure 11. Concluded.

Figure 12 shows PSDs from hot films 19, 25, and 27. A dominant flow feature is at 13 Hz seen in hot films 19 and 27 but not in hot film 25. The lack of the 13 Hz signal in hot film 25 supports the hypothesis that the boundary layer was separated in this region

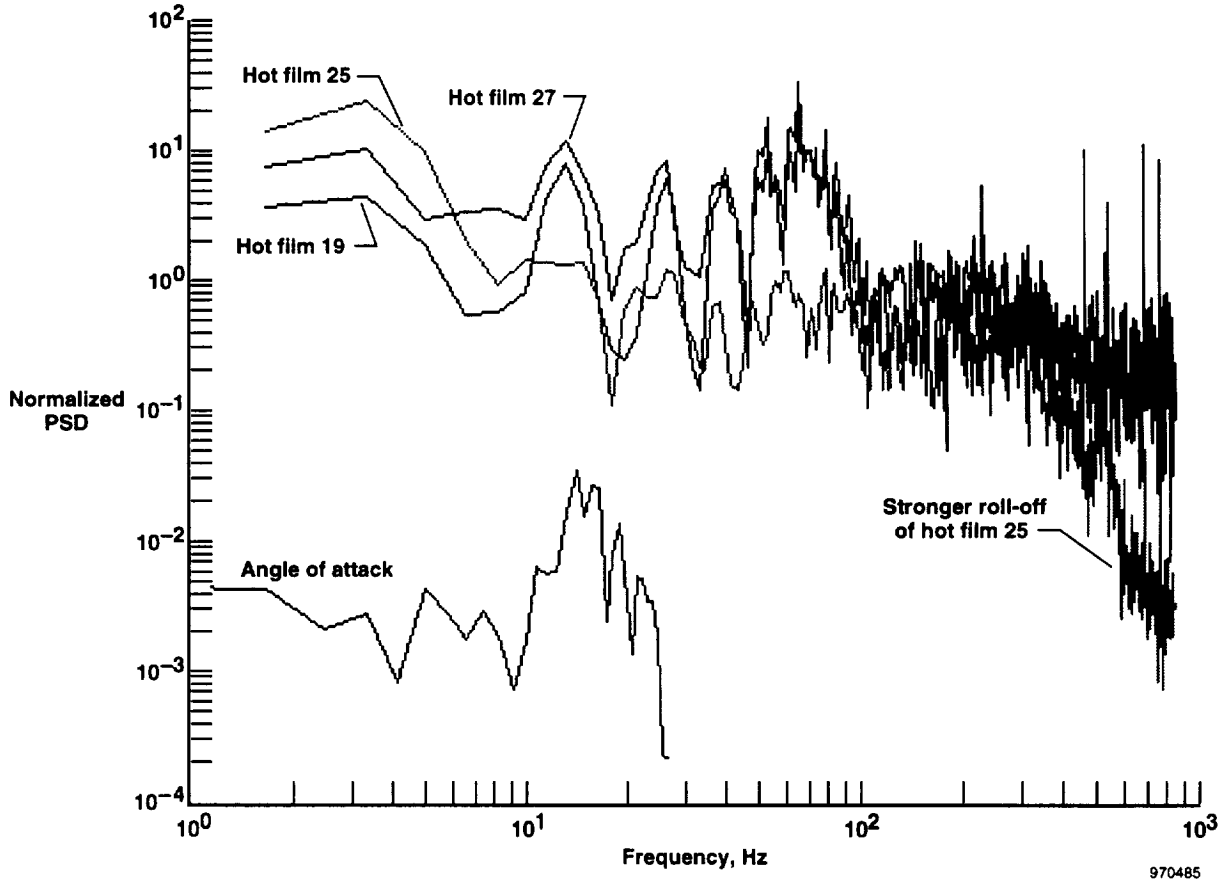

Figure 12. Power spectral densities of hot films 19, 25, and 27 and angle of attack during a stabilized test point at Mach 0.7.

and thus prevented the 13-Hz phenomena from impacting surface hot film 25. At higher frequencies the magnitude of the PSD for hot film 25 drops off more rapidly than the other signals. Tests at other Mach numbers also showed that this observation was typical of PSD magnitudes from hot films between two minimums.

Real-Time Sensor

One objective of this phase of the study was to obtain an approach for a sensor for real-time shock location. A potential approach is to identify the shock location based on the minimum mean voltage from the array of CVA outputs. As previously discussed and shown in figure 5, the hot film with the minimum mean output is near the rapid pressure rise caused by the transonic shock. A second minimum is sometimes evident slightly downstream of the first.

These two minimums were hypothesized to be the point of boundary layer flow separation induced by the shock and the reattachment point. In some cases, the hot film at the reattachment point outputs a lower voltage than the hot film at the separation point. Therefore, any algorithm using this approach would need to differentiate between these two points.

A shock location algorithm was written to analyze acceleration and angle-of-attack sweep maneuvers using the minimum mean voltage output approach. In both cases the boundary layer was laminar before the transonic shock. The shock location algorithm obtained hot-film mean voltages over 0.01-sec intervals to simulate a 100-Hz sensor output.

Figure 13 shows results from analyzing hot films 20 through 35 during a level acceleration maneuver. Figure 13(a) shows

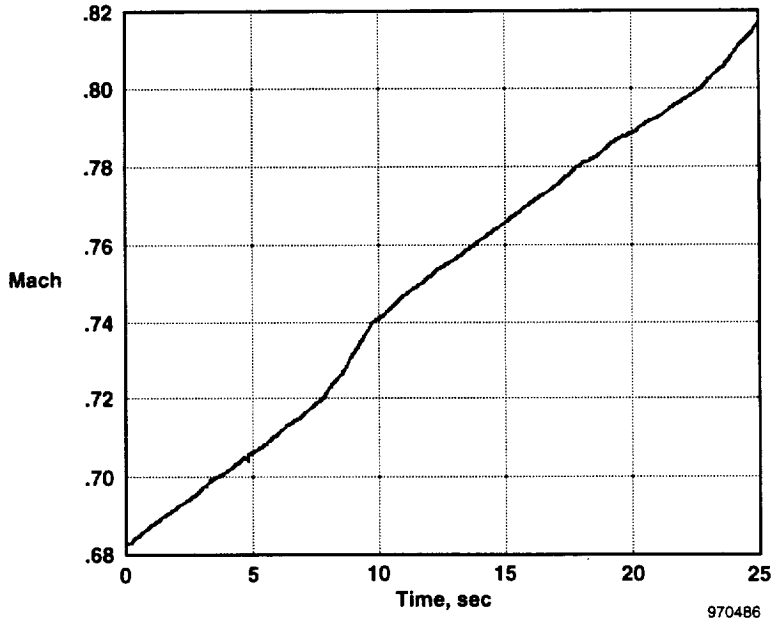

(a) Mach-number time history.

Figure 13. Time history of a level acceleration maneuver demonstrating the shock location algorithm output for a laminar flow boundary layer.

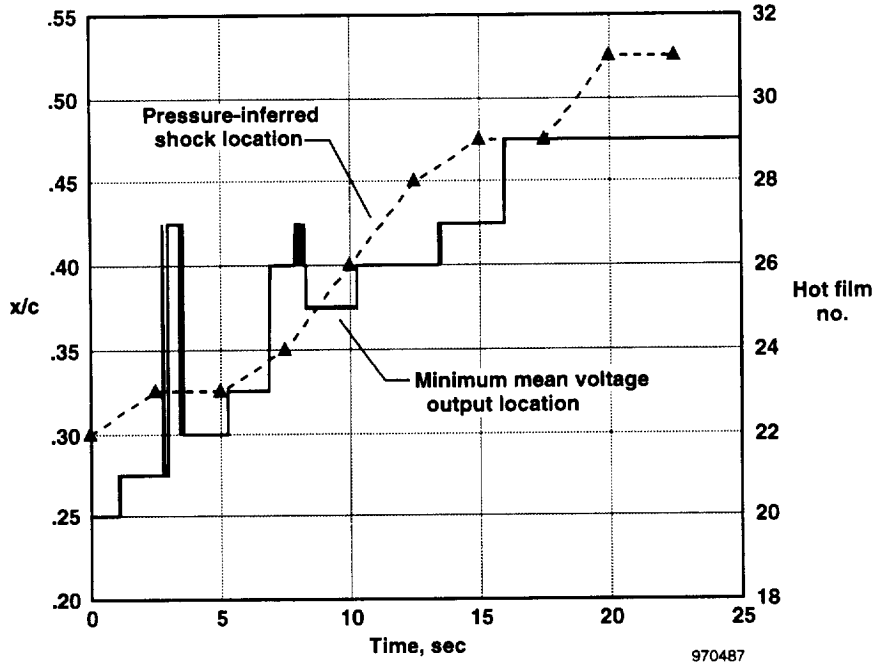

(b) Comparison of locations of the minimum mean voltage output with the pressure-inferred shock.

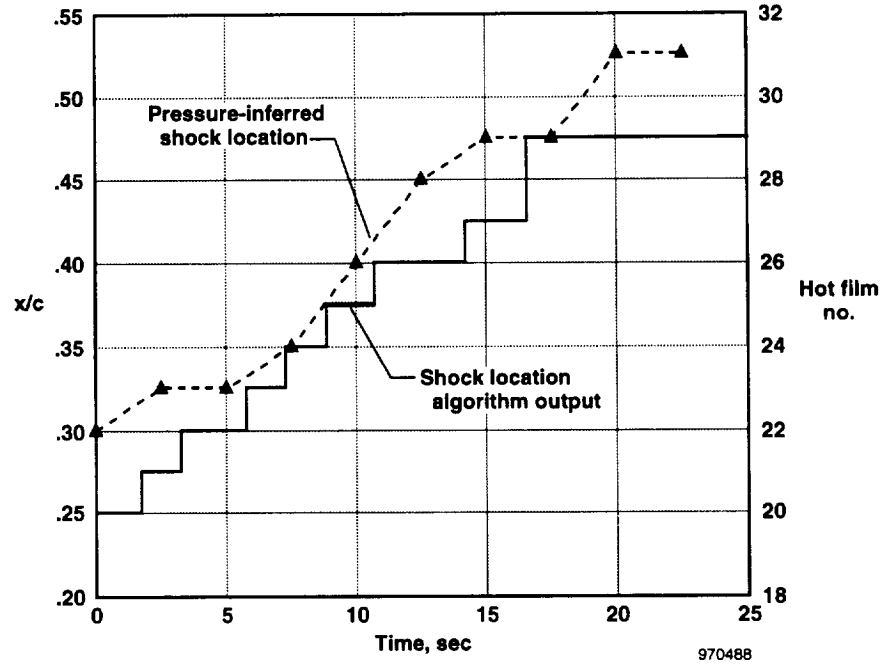

(c) Comparison of the shock location algorithm output with the pressure-inferred shock location.

Figure 13. Concluded.

the Mach time history. Figure 13(b) plots the hot film that outputs the minimum value. Figure 13(c) is a result of the shock location algorithm that chooses the forward hot film when there are two distinct minimums (as in figs. 5(a) and 5(b)).

The location of the shock inferred from the pressure measurements is also shown in figures 13(b) and 13(c). As can be seen, the shock location algorithm output consistently locates the minimum one or two hot films ahead of the inferred shock location.

The angle-of-attack sweep plotted in figure 8 was also analyzed with and without the shock location algorithm, and figures 14(a), 14(b), and 14(c) show the results. Without the shock location algorithm, there is a part of the maneuver where the minimum location oscillates between hot films 22 and 26 and stabilizes at hot film 26. The pressure-inferred shock location, however, is always before hot film 26. With the shock location algorithm, the chosen hot film is always slightly forward of the inferred shock location, as expected for the laminar flow case, and the algorithm adequately tracks the shock.

Spectral analysis, and in particular phase reversal, could also be used in real-time shock location identification (although for this study, no phase reversal algorithm results are presented). Although phase reversal can indicate the location of the shock, such reversal is not a necessary condition because phase reversal requires

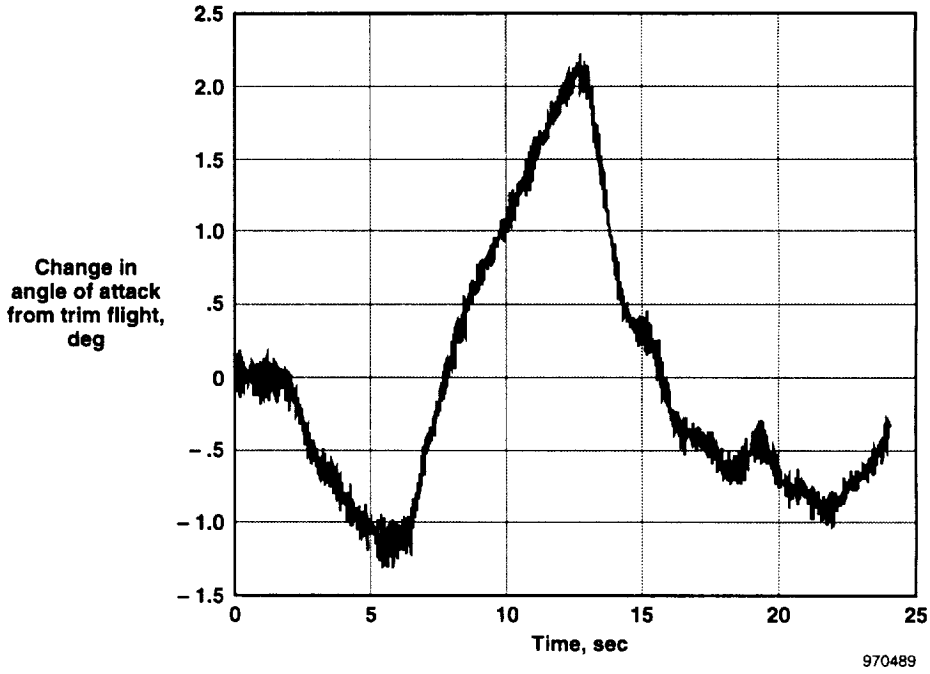

(a) Angle-of-attack time history.

Figure 14. Time history of an angle-of-attack sweep demonstrating the shock location algorithm output for a laminar flow boundary layer.

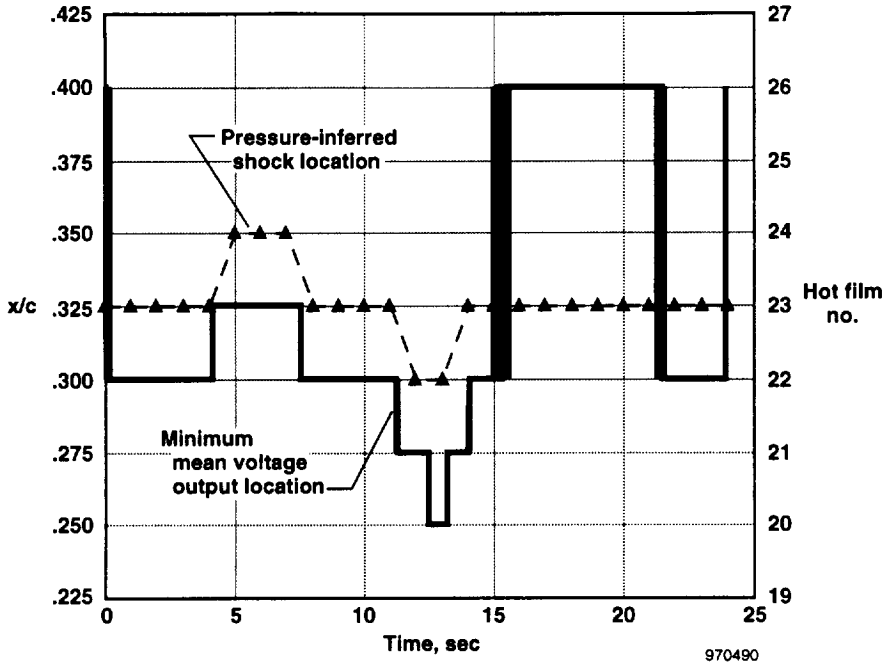

(b) Comparison of locations of the minimum mean voltage output with the pressure-inferred shock.

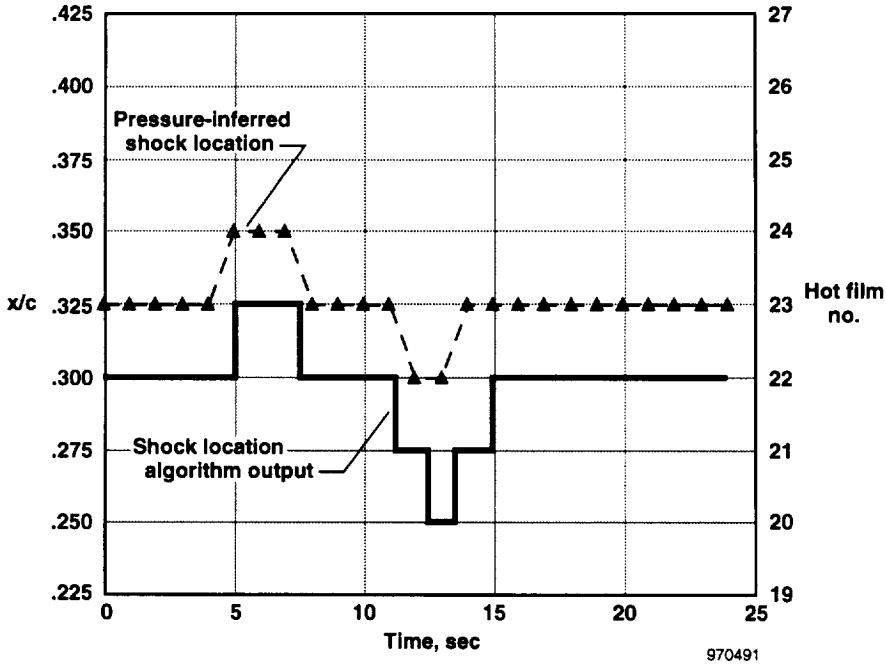

(c) Comparison of the shock location algorithm output with the pressure-inferred shock location.

Figure 14. Concluded.

oscillatory motion of the shock at a frequency higher than the desired shock location sensor output frequency.

Concluding Remarks

Flight test data were obtained from a shock location sensor comprised of hot films controlled with constant voltage anemometry. Tests were flown on the F-15B Flight Test Fixture (FTF) at NASA Dryden Flight Research Center using a modified NACA 0021 airfoil attached to the side of the FTF. Hot-film and pressure measurements were obtained along the chord of the test article.

The shock location inferred by pressure measurements was correlated with the hot-film outputs. For laminar flow upstream of the shock, the array of hot films showed a minimum output slightly upstream of the pressure-inferred shock location. For test conditions with tripped (partially turbulent) flow upstream of the shock, the array of hot films showed a minimum slightly downstream of the pressure-inferred shock location. The hot-film minimum is hypothesized to correspond to the start of a shock-induced separation bubble inside the boundary layer.

A shock location algorithm simulated 100–Hz output of a real-time sensor. Results from the algorithm were presented, showing consistent movement of the hot-film array minimum with the shock. A phase-reversal analysis was also presented in the paper. Phase reversal is a technique that can be used to locate the hot-film array minimum if the location is oscillatory.

Appendix A
Use of CVA for Shock Location Sensing

The interaction of a shock with a boundary layer increases ambient air temperature and changes the flow velocity along a surface. Surface-mounted hot films could potentially sense both of these changes. Figure A1 shows the basic CVA circuit used to control the hot films. A complete analysis of this circuit has been presented.[2]

Note that whereas the hot film is maintained at a constant voltage (V_s), the circuit output voltage (V_o) does change because of hot-film resistance changes. The output voltage change from a reference condition is related to the resistance change as

$$\Delta V_o = -R_2 I_s \left(\frac{\Delta R_s}{R_s} \right)$$

For this application, the reference condition refers to a low-speed flight condition at the test altitude in which no shock was incident on the sensor. The fractional change in the hot-film resistance is related to the change in the temperature in the hot film by

$$\frac{\Delta R_s}{R_s} = \frac{\alpha \, \Delta T}{1 + \alpha \, \Delta T}$$

where α is the temperature coefficient of resistance of the nickel hot-film material, and ΔT is the change in temperature from the reference condition. Therefore, the output voltage change due to temperature change is

$$\Delta V_o = -R_2 I_s \left(\frac{\alpha \, \Delta T}{1 + \alpha \, \Delta T} \right)$$

All hot films in the array were made from the same sheet of nickel film, and therefore they had the same temperature coefficient of resistance α of approximately 0.004 Ω/Ω/°C. R_2 is a circuit constant that is a precision resistor (±0.1 percent tolerance). I_s varies as the hot-film temperature changes; however, it was initially set at the low-speed reference condition such that the sensitivity factor, $R_2 I_s$, was identical for each hot film in the array at the reference condition.

Figure A2 shows a schematic of the operation of the CVA system. This

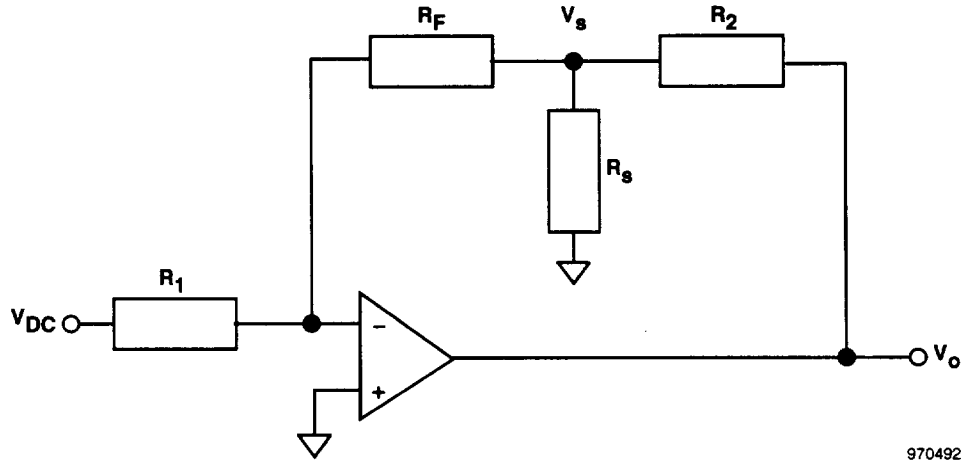

Figure A1. Basic CVA circuit (U.S. Patent 5074147).

arrangement was designed to obtain highly discernible voltage outputs from the hot-film temperature changes. At the stabilized low-speed reference flight condition, the aircraft pilot toggled the CVA Reset switch, which started the Auto Current Control sequence. This sequence set the hot-film current levels such that the sensitivity factor $R_2 I_s$ would be identical in each hot-film CVA circuit.

After completion of the Auto Current Control sequence, the pilot toggled the Auto Zero switch. This configured the Auto Zero unit to subtract the static output voltage (V_o) measured at the reference condition from the CVA outputs. This step was necessary because the static output voltage (V_o) could be as large as 15 V for a 100-mA current through the hot film. The voltage changes resulting from the shock, however, were only tenths of volts. To discern these changes with higher resolution, the static V_o measured at the reference condition was removed from the measured output.

The CVA has been shown to be sensitive primarily to ambient temperature changes at low-current (low-overheat) levels and sensitive primarily to velocity fluctuations at high-current (high-overheat) levels.[7] Flight tests at low-current levels (I_s ~ 30 mA) were largely unsuccessful in producing CVA outputs that correlated well with the pressure-inferred shock locations. Flight tests at high-current levels (I_s ~ 100 mA), however, produced CVA outputs that did correlate well with the pressure-inferred shock location.

This result suggests that the primary effect of the shock on the hot films was to change the convective heat transfer caused by the velocity fluctuations in the boundary layer. Consequently, high-current levels were used for the results presented in this paper.

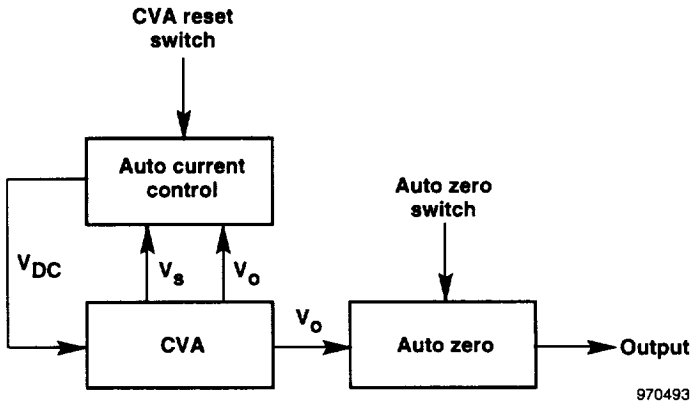

Figure A2. CVA and Auto-Zero arrangement.

Appendix B
Phase Reversal Illustration

Phase reversal between hot films can be used as an indicator of shock location. The phase-reversal phenomena is explained using figure B1(a), which graphs hypothetical voltage outputs from eight hot-film sensors at five time points. In this figure, we assume that the shock location is identified by the minimum voltage output. At the initial time, the shock is located at sensor S4. As time changes, the shock moves between sensors S5, S4, and S3 as indicated by the black dot.

Figure B1(b) shows the time histories for each of the sensors. As can be seen, sensors S1, S2, and S3 are in phase with each other. Sensors S5, S6, S7, and S8 are also in phase with each other. However, these two groups of sensors are completely out of phase with each other. Furthermore, sensor S4 varies at twice the frequency of the other sensors.

Hence, if the shock is oscillating about a particular hot film, we would expect to see a phase reversal between hot films on either side of that particular hot film. We would also expect to see the particular hot film about which the shock is oscillating to exhibit a frequency twice the oscillation frequency.

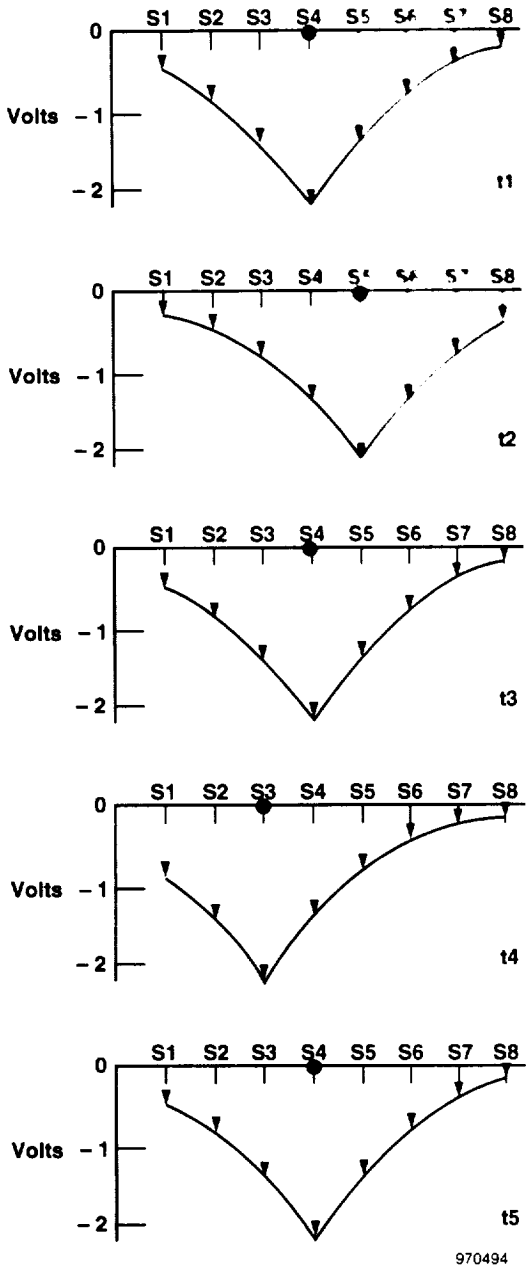

B1(a) Output voltage as a function of sensor at five points in time.

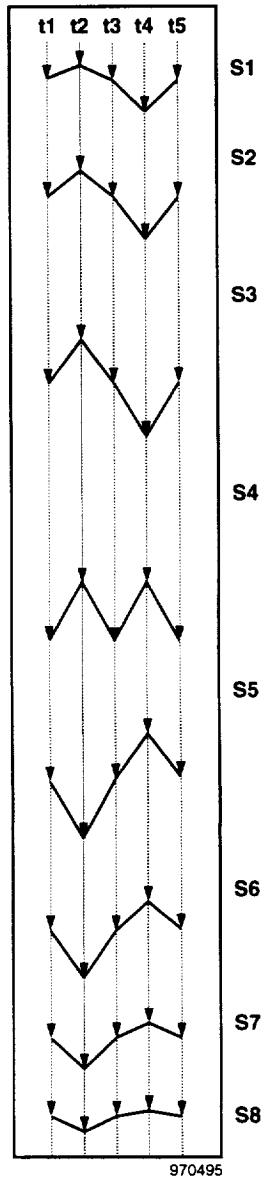

B1(b) Output voltage as a function of time at eight sensor locations.

Figure B1. Phase reversal illustration.

References

[1]Loving, Donald L., *Wind-Tunnel—Flight Correlation of Shock-Induced Separated Flow*, NASA TN D-3580, Sept. 1966.

[2]Sarma, Garimella R., "Analysis of a Constant Voltage Anemometer Circuit," IEEE Instrumentation and Measurement Technology Conference, Irvine, California, May 1993.

[3]Mangalam, S. M., G. R. Sarma, S. Kuppa, and L. R. Kubendran, "A New Approach to High-Speed Flow Measurements Using Constant Voltage Anemometry," AIAA-92-3957, July 1992.

[4]Mangalam, S. M., G. R. Sarma, and S. Kuppa, "Quantitative Flow Diagnostics Techniques for Unsteady Aerodynamics," 2nd Pacific International Conference on Aerospace Science & Technology, Melbourne, Australia, Mar. 1995.

[5]Harvey, Don, Subrahmanyam Kuppa, Garimella R. Sarma, and Siva M. Mangalam, "Demonstration of the Constant Voltage Anemometer (CVA) in the National Transonic Facility (NTF)," ASME, Aug. 1995.

[6]Harvey, Don, S. Kuppa, Daryl Sinclair, and Kurt Lotter, "Demonstration of an Advanced Flow Diagnostics System in the AEDC 16T," AIAA-95-2833, July 1995.

[7]Kegerise, Michael A. and Eric F. Spina, "A Comparative Study of Constant-Voltage and Constant-Temperature Hot-Wire Anemometers in Supersonic Flow," 3rd International Symposium on Thermal Anemometry, July 1996.

[8]Abbot, Ira H. and Albert E. Von Doenhoff, *Theory of Wing Sections*, Dover Publications, Inc., New York, 1958.

[9]Richwine, David M., *F-15B/Flight Test Fixture II: A Test Bed for Flight Research*, NASA TM-4782, Dec. 1996.

[10]Shapiro, Ascher H., *The Dynamics and Thermodynamics of Compressible Fluid Flow*, The Roland Press Company, New York, 1954.

[11]Schlichting, Hermann, *Boundary-Layer Theory*, seventh edition, McGraw-Hill Book Company, 1979.

[12]Pearcey, H. H. and D. W. Holder, "Examples of the Effects of Shock-Induced Boundary-Layer Separation in Transonic Flight," Ministry of Technology, Aeronautical Research Council, R. & M. No. 3510, Jan. 1954.

[13]Seddon, J. and E. L. Goldsmith, *Intake Aerodynamics*, AIAA Education Series, AIAA and BSP Professional Books, 1985.

[14]Delery, J. and J. G. Marvin, "Shock-Wave Boundary Layer Interactions," AGARDograph No. 280, Feb. 1986.

REPORT DOCUMENTATION PAGE

Form Approved
OMB No. 0704-0188

1. AGENCY USE ONLY (Leave blank)	2. REPORT DATE	3. REPORT TYPE AND DATES COVERED
	August 1997	Technical Memorandum

4. TITLE AND SUBTITLE

Flight Demonstration of a Shock Location Sensor Using Constant Voltage Hot-Film Anemometry

5. FUNDING NUMBERS

WU 529 21 34 00 38 00 F15

6. AUTHOR(S)

Timothy R. Moes, Garimella R. Sarma, and Siva M. Mangalam

7. PERFORMING ORGANIZATION NAME(S) AND ADDRESS(ES)

NASA Dryden Flight Research Center
P.O. Box 273
Edwards, California 93523-0273

8. PERFORMING ORGANIZATION REPORT NUMBER

H-2191

9. SPONSORING/MONITORING AGENCY NAME(S) AND ADDRESS(ES)

National Aeronautics and Space Administration
Washington, DC 20546-0001

10. SPONSORING/MONITORING AGENCY REPORT NUMBER

TM-4806

11. SUPPLEMENTARY NOTES

Presented at the 1997 Society of Flight Test Engineers Symposium, Orlando, Florida, August 18-22, 1997. Timothy R. Moes, Dryden Flight Research Center, Edwards, California; Garimella R. Sarma, and Siva M. Mangalam, Tao of Systems Integration, Inc., Hampton, Virginia.

12a. DISTRIBUTION/AVAILABILITY STATEMENT

Unclassified—Unlimited
Subject Category 06

12b. DISTRIBUTION CODE

13. ABSTRACT (Maximum 200 words)

Flight tests have demonstrated the effectiveness of an array of hot-film sensors using constant voltage anemometry to determine shock position on a wing or aircraft surface at transonic speeds. Flights were conducted at the NASA Dryden Flight Research Center using the F-15B aircraft and Flight Test Fixture (FTF). A modified NACA 0021 airfoil was attached to the side of the FTF, and its upper surface was instrumented to correlate shock position with pressure and hot-film sensors. In the vicinity of the shock-induced pressure rise, test results consistently showed the presence of a minimum voltage in the hot-film anemometer outputs. Comparing these results with previous investigations indicate that hot-film anemometry can identify the location of the shock-induced boundary layer separation. The flow separation occurred slightly forward of the shock-induced pressure rise for a laminar boundary layer and slightly aft of the start of the pressure rise when the boundary layer was tripped near the airfoil leading edge. Both minimum mean output and phase reversal analyses were used to identify the shock location.

14. SUBJECT TERMS	15. NUMBER OF PAGES
Transonic Shocks, Shock Impingement, Boundary Layers, Hot-Films, Anemometry, Constant Voltage Anemometry	28
	16. PRICE CODE A03

17. SECURITY CLASSIFICATION OF REPORT	18. SECURITY CLASSIFICATION OF THIS PAGE	19. SECURITY CLASSIFICATION OF ABSTRACT	20. LIMITATION OF ABSTRACT
Unclassified	Unclassified	Unclassified	Unlimited